

QUANTUM DOT DETECTORS WITH PLASMONIC STRUCTURES

Sanjay Krishna

**University of New Mexico
1313 Goddard SE
Albuquerque, NM 87106**

15 May 2015

Final Report

APPROVED FOR PUBLIC RELEASE; DISTRIBUTION IS UNLIMITED.



**AIR FORCE RESEARCH LABORATORY
Space Vehicles Directorate
3550 Aberdeen Ave SE
AIR FORCE MATERIEL COMMAND
KIRTLAND AIR FORCE BASE, NM 87117-5776**

DTIC COPY NOTICE AND SIGNATURE PAGE

Using Government drawings, specifications, or other data included in this document for any purpose other than Government procurement does not in any way obligate the U.S. Government. The fact that the Government formulated or supplied the drawings, specifications, or other data does not license the holder or any other person or corporation; or convey any rights or permission to manufacture, use, or sell any patented invention that may relate to them.

This report is the result of contracted fundamental research deemed exempt from public affairs security and policy review in accordance with SAF/AQR memorandum dated 10 Dec 08 and AFRL/CA policy clarification memorandum dated 16 Jan 09. This report is available to the general public, including foreign nationals. Copies may be obtained from the Defense Technical Information Center (DTIC) (<http://www.dtic.mil>).

AFRL-RV-PS-TR-2015-0102 HAS BEEN REVIEWED AND IS APPROVED FOR
PUBLICATION IN ACCORDANCE WITH ASSIGNED DISTRIBUTION STATEMENT.

//SIGNED//
DAVID CARDIMONA
Program Manager

//SIGNED//
PAUL D. LEVAN, Ph.D.
Technical Advisor, Space Based Advanced Sensing
and Protection

//SIGNED//
JOHN BEAUCHEMIN
Chief Engineer, Spacecraft Technology Division
Space Vehicles Directorate

This report is published in the interest of scientific and technical information exchange, and its publication does not constitute the Government's approval or disapproval of its ideas or findings.

REPORT DOCUMENTATION PAGE				Form Approved OMB No. 0704-0188	
Public reporting burden for this collection of information is estimated to average 1 hour per response, including the time for reviewing instructions, searching existing data sources, gathering and maintaining the data needed, and completing and reviewing this collection of information. Send comments regarding this burden estimate or any other aspect of this collection of information, including suggestions for reducing this burden to Department of Defense, Washington Headquarters Services, Directorate for Information Operations and Reports (0704-0188), 1215 Jefferson Davis Highway, Suite 1204, Arlington, VA 22202-4302. Respondents should be aware that notwithstanding any other provision of law, no person shall be subject to any penalty for failing to comply with a collection of information if it does not display a currently valid OMB control number. PLEASE DO NOT RETURN YOUR FORM TO THE ABOVE ADDRESS.					
1. REPORT DATE (DD-MM-YY) 15-05-2015		2. REPORT TYPE Final Report		3. DATES COVERED (From - To) 14 Nov 2011 – 17 Mar 2013	
4. TITLE AND SUBTITLE Quantum Dot Detectors with Plasmonic Structures				5a. CONTRACT NUMBER FA9453-12-1-0131	
				5b. GRANT NUMBER	
				5c. PROGRAM ELEMENT NUMBER 63401F	
6. AUTHOR(S) Sanjay Krishna				5d. PROJECT NUMBER 2181	
				5e. TASK NUMBER PPM00015934	
				5f. WORK UNIT NUMBER EF125031	
7. PERFORMING ORGANIZATION NAME(S) AND ADDRESS(ES) University of New Mexico 1313 Goddard SE Albuquerque, NM 87106				8. PERFORMING ORGANIZATION REPORT NUMBER	
9. SPONSORING / MONITORING AGENCY NAME(S) AND ADDRESS(ES) Air Force Research Laboratory Space Vehicles Directorate 3550 Aberdeen Ave., SE Kirtland AFB, NM 87117-5776				10. SPONSOR/MONITOR'S ACRONYM(S) AFRL/RVSS	
				11. SPONSOR/MONITOR'S REPORT NUMBER(S) AFRL-RV-PS-TR-2015-0102	
12. DISTRIBUTION / AVAILABILITY STATEMENT Approved for public release; distribution is unlimited.					
13. SUPPLEMENTARY NOTES					
14. ABSTRACT Objective is to investigate the design, fabrication, and characterization, of multi-spectral quantum dots-in-a-double well (DDWELL) infrared detectors, by the integration of a surface Plasmon (SP) assisted resonant cavity with the infrared detectors.					
15. SUBJECT TERMS plasmonic, infrared, detectors, resonant cavity					
16. SECURITY CLASSIFICATION OF:			17. LIMITATION OF ABSTRACT	18. NUMBER OF PAGES	19a. NAME OF RESPONSIBLE PERSON
a. REPORT	b. ABSTRACT	c. THIS PAGE			David Cardimona
Unclassified	Unclassified	Unclassified	Unlimited	20	19b. TELEPHONE NUMBER (include area code)

(This page intentionally left blank)

TABLE OF CONTENTS

SECTION	PAGE
List of Figures.....	ii
List of Tables.....	ii
1. SUMMARY.....	1
2. INTRODUCTION.....	1
3. METHODS, ASSUMPTIONS, AND PROCEDURES.....	2
4. RESULTS AND DISCUSSIONS	3
5. CONCLUSIONS.....	8
REFERENCES.....	9
LIST OF ABBREVIATIONS.....	11

LIST OF FIGURES

FIGURES	PAGE
1. Structure of 2D-Au-CHA integrated DWELL based back-illuminated infrared photodetector.....	4
2. Absorption calculated in the different layers of the 2D-Au-CHA:DWELL FPA as a function of the illumination wavelength	5
3. Simulated responsivities of the DWELL FPA (gray square), 2D-Au-CHA:DWELL FPA (black square) and enhancement ratio (red circle) resulting from 2D-Au-CHA, i.e, R2D-Au-CHA:DWELL FPA/RDWELL FPA.....	6
4. Experimental SNRs of the DWELL FPA (gray triangle) and 2D-Au-CHA:DWELL FPA (black triangle), and the corresponding enhancement ration (red diamond) by 2D-AU-CHA:DWELL FPA over the DWELL FPA.....	7

LIST OF TABLES

TABLES	PAGE
1. Table showing that all the four tasks proposed were completed.....	2

ACKNOWLEDGMENTS

This work was supported by the Korea Research Institute of Standards and Science under the project “Study of infrared surface plasmon resonance for optical enhancement and wavelength tuning”, grant JP2012-0001 and is based on research sponsored by Air Force Research Laboratory under agreement number FA9453-12-1-0131. The U.S. Government is authorized to reproduce and distribute reprints for Governmental purposes notwithstanding any copyright notation thereon.

DISCLAIMER

The views and conclusions contained herein are those of the authors and should not be interpreted as necessarily representing the official policies or endorsements, either expressed or implied, of Air Force Research Laboratory or the U.S. Government.

(This page intentionally left blank)

1. SUMMARY

Objective and Proposed Approach

The goal of this project was to investigate the design, fabrication, and characterization, of multi-spectral quantum dots-in-a-double well (DDWELL) infrared detectors and investigate the integration of a Surface Plasmon (SP) assisted resonant cavity with the infrared detectors. Multicolor detector capabilities are highly desirable for advanced IR imaging systems, since they provide enhanced target discrimination and identification, combined with lower false-alarm rates. Systems that collect data in separate IR spectral bands can discriminate both absolute temperature as well as unique signatures of objects in the scene. By providing this new dimension of contrast, multiband detection also offers advanced color processing algorithms to further improve sensitivity above that of single-color devices. This is extremely important for identifying temperature differences between missile targets, warheads, and decoys. Multispectral IR focal plane arrays (FPAs) are highly beneficial for a variety of applications such as missile warnings guidance, precision strike, airborne surveillance, target detection, and recognition. Military surveillance, target detection, and target tracking can be undertaken using single-color FPAs if the targets are easy to identify. However, in the presence of clutter, or when the target and/or background are uncertain, or in situations where the target and/or background may change during engagement, single-color system design involves compromises that can degrade overall capability. It is well established that in order to reduce clutter and enhance the desired features' contrast, one will require the use of multispectral focal plane arrays. In such cases, multicolor imaging can greatly improve overall system performance.

The focus of this one year effort was to undertake a trade study to evaluate these technologies and a rigorous investigation of the performance parameters of these technologies.

2. INTRODUCTION

Intellectual Impact

Plasmonic structures were integrated with quantum dot detectors with enhancement using a back-side illuminated geometry. Two peer reviewed publications resulted from this work.¹

Personnel Impact

One of the graduate students working on this project (Woo-Yang Jang) successfully defended his PhD and is currently employed at the Air Force Research Laboratory. One other student (Ajit Barve) who provided material support for this project also defended his PhD and is currently at the University of California, Santa Barbara.

¹ (i) Z. Ku, W.-Y. Jang, J. Zhou, J. O. Kim, A. V. Barve, S. Silva, S. Krishna, S. R. J. Brueck, R. Nelson, A. Urbas, S. Kang, and S. J. Lee, "Analysis of subwavelength metal hole array structure for the enhancement of back-illuminated quantum dot infrared photodetectors," *Opt. Exp.*, **21**, pp 4709-4716 (2013).

(ii) Y. D. Sharma, Y. C. Jun, J. O. Kim, I. Brener, and S. Krishna, "Polarization-dependent Photocurrent Enhancement in Metamaterial-integrated Quantum Dot Infrared Detectors," *Opt. Comm.* **312**, pp 31-34 (2014).

3. METHODS, ASSUMPTIONS, AND PROCEDURES

Statement of Work and Milestones

The key tasks for this research program were:

Task 1: Design and growth optimization of quantum dots (QD) heterostructures

Task 2: Investigation of Surface Plasmon (SP)

Task 3: Growth and characterization of single pixel detectors

Task 4: Development and characterization of back side illuminated devices.





Task	Q1	Q2	Q3	Q4
Task 1				
Task 2				
Task 3				
Task 4				

Table 1. Table showing that all the four tasks proposed were completed.

Detailed Technical Discussion

The impact of a two-dimensional metal hole array structure integrated to the back-illuminated quantum dots-in-a-well (DWELL) infrared photodetectors was investigated. The metal hole array consisting of subwavelength-circular holes penetrating gold layer (2D-Au-CHA) provides the enhanced responsivity of DWELL infrared photodetector at certain wavelengths. The performance of 2D-Au-CHA is investigated by calculating the absorption of active layer in the DWELL structure using a finite integration technique. Simulation results show that the performance of the DWELL focal plane array (FPA) is improved by enhancing the coupling to active layer via local field engineering resulting from a surface plasmon polariton mode and a guided Fabry-Perot mode. The simulation method accomplished in this paper provides a generalized approach to optimize the design of any type of couplers integrated to infrared photodetectors. Experimental results demonstrate the enhanced signal-to-noise ratio by the 2D-Au-CHA integrated FPA as compared to the DWELL FPA. A comparison between the experiment and the simulation shows a good agreement.

In the past decade, the infrared detectors based on intersubband transitions in quantum dots (QDs) have attracted much attention due to lower dark currents and increased lifetimes compared with quantum well infrared photodetectors, which are in turn due to three-dimensional confinement and the reduction of scattering, respectively [1, 2]. These epitaxially self-assembled and nanometer-scale QD islands form spontaneously on a semiconductor substrate because of lattice mismatch [3]. More recently, infrared detectors based on QDs embedded in a quantum

well (QW), known as dots-in-a-well (DWELL) heterostructure, have been proposed [4]. The DWELL architecture brings the advantages of QWs, such as control over the operating wavelength, while maintaining the advantages of QDs, such as normal incidence operation [5]. In parallel, focal plane array (FPA) development for infrared imaging has proceeded from the first to third generations (linear arrays, 2D arrays for staring systems, and large format with enhanced capabilities, respectively). For a step closer to the next generation of FPAs, we envision that perforated metal film structures [6, 7] will improve the performance of FPA by enhancing the coupling to photodetectors via local field engineering, and will enable spectral sensitivity modifications. In regard to the improved performance at certain wavelengths, it is worth pointing out the structural difference between previous perforated metal film integrated front-illuminated single pixel devices [8–10] and our back-illuminated device (FPA) [11]. Apart from the pixel linear dimension, it is a distinct difference that there is a metal cladding (composed of a number of metals for ohmic contact and within the read-out integrated circuit) in the FPA between the heavily doped gallium arsenide (GaAs) used as the contact layer and the read-out integrated circuit (i.e., n-type GaAs/QD-absorber/n-type GaAs/metal cladding). On the contrary, the front-illuminated single pixel device consists of two heavily doped contact layers separated by the QD-absorber on a semi-infinite GaAs substrate (i.e., n-type GaAs/QD-absorber/n-type GaAs/substrate).

In this work, a single metal layer is chosen as the metal cladding in the simulation to allow clearer demonstration of the effects of a two-dimensional square array of circular holes in Au layer (2D-Au-CHA). As a result of the 2D-Au-CHA and metal ground plane, the 2D-Au-CHA integrated DWELL FPA (2D-Au-CHA:DWELL FPA) yields a wavelength selective resonant enhancement of the detector response in the mid-infrared spectral region. The analysis and comparison of modeling results with experiment indicates a good quantitative agreement of the improved performance of DWELL FPA measured using the signal to noise (SNR) and the noise equivalent difference in temperature (NEDT) at resonance wavelengths. The improved performance results from a surface plasmon polariton (SPP) mode and a guided Fabry-Perot mode, that enhance x or y (along the polarization direction used in simulation) and z (along the growth direction) components of electric field in the active region compared with the unmodified DWELL FPA at certain wavelengths.

4. RESULTS AND DISCUSSION

In order to find the optimum dimension of 2D-Au-CHA to match the first order SPP resonance with the maximum of DWELL FPA's spectral response, we employed both the commercial software (Computer Simulation Technology's Microwave Studio: Computer Simulation Technology GmbH, Darmstadt, Germany)² based on a finite integration technique and a rigorous coupled wave analysis [12]. Comparable results were obtained for both techniques (not shown here).

Indium arsenide (InAs) QDs were grown with VG-80 solid source molecular beam epitaxy (MBE) system using a Stranski–Krastanow growth mode [13]. After the MBE growth, the FPA was fabricated (a dry etch to form the mesa, surface passivation (SiNx), ohmic metal

² www.cst.com

evaporation, under bump metallization, indium deposition, and indium reflow process) and then hybridized to the read-out integrated circuit by flip-chip bonding processing. Following the removal of substrate and AlAs etch stop layer, the 2D-Au-CHA was fabricated on a 1 μm thick contact layer of the DWELL FPA as shown in Fig. 1(a)

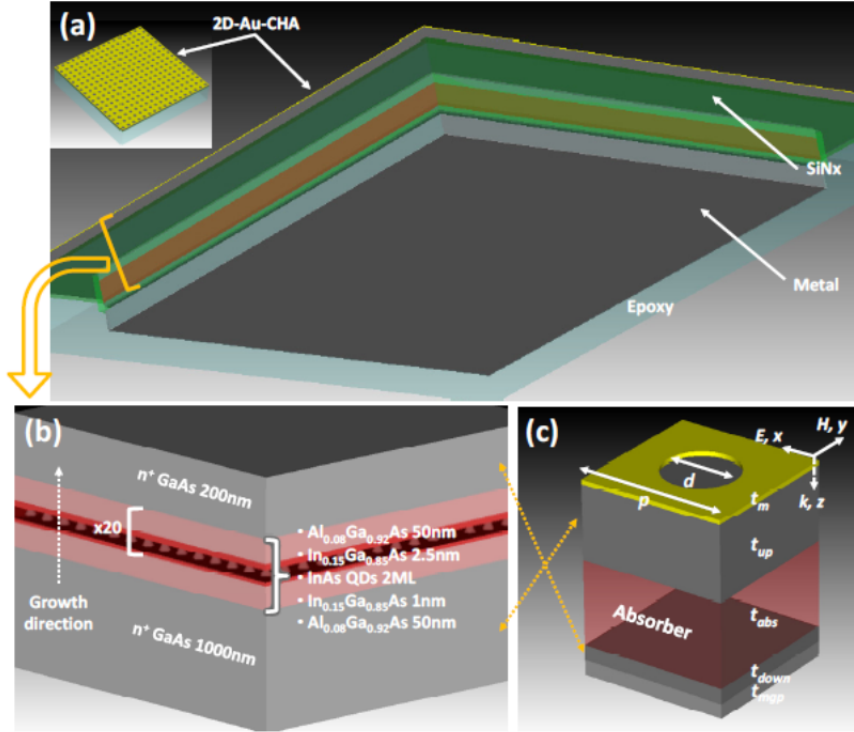


Fig. 1 Structure of 2D-Au-CHA integrated DWELL based back-illuminated infrared photodetector

The schematic diagram in Fig. 1(a) illustrates a pixel in the 2D-Au-CHA:DWELL FPA (after substrate and AlAs etch stop layer were removed). The zoomed-in image in Fig. 1(b) depicts the DWELL heterostructure within a pixel. The DWELL structure includes the n-doped GaAs contact layers with 200/1000 nm thicknesses, the active region with 20 stacks of InAs QDs embedded in 3.5 nm thick In_{0.15}Ga_{0.85}As/Al_{0.08}Ga_{0.92}As QWs, each separated by 50 nm thick Al_{0.08}Ga_{0.92}As barriers. Figure 1(c) shows geometrical parameters of a simplified unit cell of the 2D-Au-CHA:DWELL FPA used for numerical simulation. The details of MBE growth/fabrication of DWELL FPA and 2D-Au-CHA are : $p = 1.8 \mu\text{m}$; $d = p/2$; $t_m = 50 \text{ nm}$; $t_{up} = 1 \mu\text{m}$; $t_{abs} = 1.12 \mu\text{m}$; $t_{down} = 0.2 \mu\text{m}$; $t_{mcp} = 0.2 \mu\text{m}$. In addition, the configuration of polarization and propagation is depicted (E , H , and k denote electric field, magnetic field, and wave vector, respectively) are available in Ref [11, 14].

With simulated absorption, responsivity and enhancement ratio for the purpose of understanding our experimental results quantitatively and qualitatively, we performed 3D full field electromagnetic simulations of 2D-Au-CHA:DWELL FPA using a finite integration technique. The boundary conditions on the faces (of a single cubic unit cell) parallel to the propagation

vector were set as perfect magnetic/electric conductor to approximate a transverse electromagnetic plane wave propagating through 2D-Au-CHA:DWELL FPA as shown in Fig. 1(c). All geometrical parameters are indicated in Fig. 1(c). For materials constituting 2D-Au-CHA:DWELL FPA, a Drude model was applied for the dielectric parameters of Au [15] (1.4 times larger scattering frequency than bulk Au to fit the experimental values obtained from Sandia National Laboratory), n-type GaAs [9] ($2 \times 10^{18} \text{ cm}^{-3}$) and lossy aluminium [16] used as 2D-Au-CHA, contact layer and metal ground plane, respectively. Figures 1(b) and 1(c) show that 20 stacks of QD layers were simplified to an effective absorber layer whose n_{eff} and k_{eff} (real and imaginary parts of refractive index in effective absorber) were taken from Ref [9], measured quantum efficiency [17], and spectral photoresponse.

The absorption in the active layer (or effective absorber) is only useful to determine how much the response (e.g., photocurrent, responsivity, or SNR) is enhanced with 2D-Au-CHA, i.e., the absorption of other layers is parasitic. The power absorbed per unit volume can be calculated from the divergence of the Poynting vector ($\nabla \cdot \mathbf{S} \rightarrow$) and is equivalent to $\omega \varepsilon''(\lambda) |\mathbf{E}(\lambda)|^2$, where ω is the angular frequency ($2\pi c/\lambda$), c is the speed of light in vacuum, $\varepsilon''(\lambda)$ is the imaginary part of dielectric permittivity, and $|\mathbf{E}(\lambda)|^2$ is the intensity of the electric field [18]. Therefore, the absorption in one of the layers constituting 2D-Au-CHA:DWELL FPA is calculated by $\int \omega \varepsilon''_i(\lambda) |\mathbf{E}_i(\lambda)|^2 dV_i$, where $i = \text{2D-Au-CHA, contact layers, effective absorber or metal ground plane}$. However, the absorption in effective absorber should be calculated carefully because the QD based infrared photodetector shows different response [3] depending on the orientation of electric field intensity ($|\mathbf{E}_x|^2$, $|\mathbf{E}_y|^2$, or $|\mathbf{E}_z|^2$). More specifically, the effective absorber's absorption due to 2D-Au-CHA is

$$A_{\text{2D-Au-CHA}} = \int \omega \varepsilon'' E_A(\lambda) \cdot [|\mathbf{E}_x E_A(\lambda)|^2 + \eta |\mathbf{E}_z E_A(\lambda)|^2] dV \quad (1)$$

where, $|\mathbf{E}_j E_A|^2$ is the intensity of j component-electric field in the effective absorber and ~ 8 is used for η (electric field along the growth direction shown in Fig. 1(b) is dominant in interacting with the QDs as compared to the electric field parallel to the perforated metal film) [19]. Figure 2 shows the calculated absorption in each layer of the considered 2D-Au-CHA:DWELL FPA (calculated absorption of DWELL FPA is not shown here).

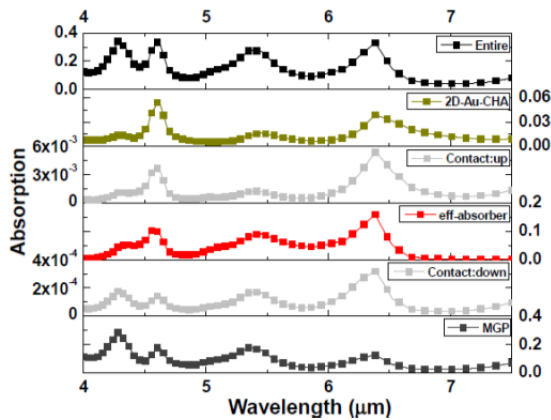


Fig. 2 Absorption calculated in the different layers of the 2D-Au-CHA:DWELL FPA as a function of the illumination wavelength.

Both DWELL FPA and 2D-Au-CHA:DWELL FPA are illuminated under the blackbody at 423K (the temperature used for measurements [11]). Using the absorption in the effective absorber as shown in Fig. 2, we calculate the responsivity (R), $R_k(\lambda) = A_k \cdot R_{BB}$ at 423K, where k is 2D-Au-CHA:DWELL FPA (or DWELL FPA), R_{BB} at 423K can be evaluated using Planck's law for the blackbody at 423 K and the equivalent spectral current density, $J(\lambda) = e N_0(\lambda)$. $N_0(\lambda)$ is the incident photon flux and e is the electron charge. Here, it is assumed that an electron-hole pair is collected for each photon absorbed in effective absorber, which corresponds to an internal quantum efficiency equal to 1.

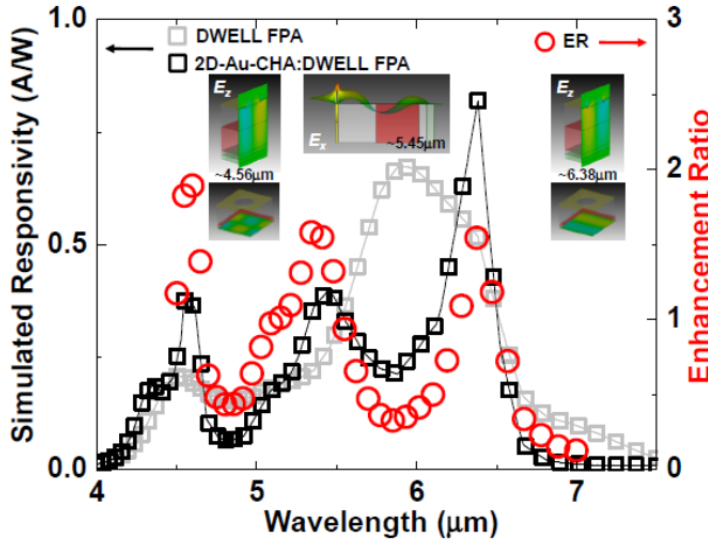


Fig. 3 Simulated responsivities of the DWELL FPA (gray square), 2D-Au-CHA:DWELL FPA (black square) and enhancement ratio (red circle) resulting from 2D-Au-CHA, i.e., $R_{2D-Au-CHA:DWELL FPA} / R_{DWELL FPA}$.

Note that unity internal quantum efficiency in effective absorbing layer is used. The simulated electric field distributions at the corresponding resonances (resulting from surface plasmon polariton and guided Fabry-Perot modes) are shown in the inset to Fig. 3. This figure also shows the simulated responsivities of DWELL FPA and 2D-Au-CHA:DWELL FPA. Moreover, in order to estimate the influence of the 2D-Au-CHA on the enhancement of the DWELL FPA efficiency, we illustrate in Fig. 3 the ratio between the responsivity of 2D-Au-CHA:DWELL FPA over the responsivity of DWELL FPA, which is represented by the red circle and agrees well with the SNR measurements as will be shown in Fig. 4

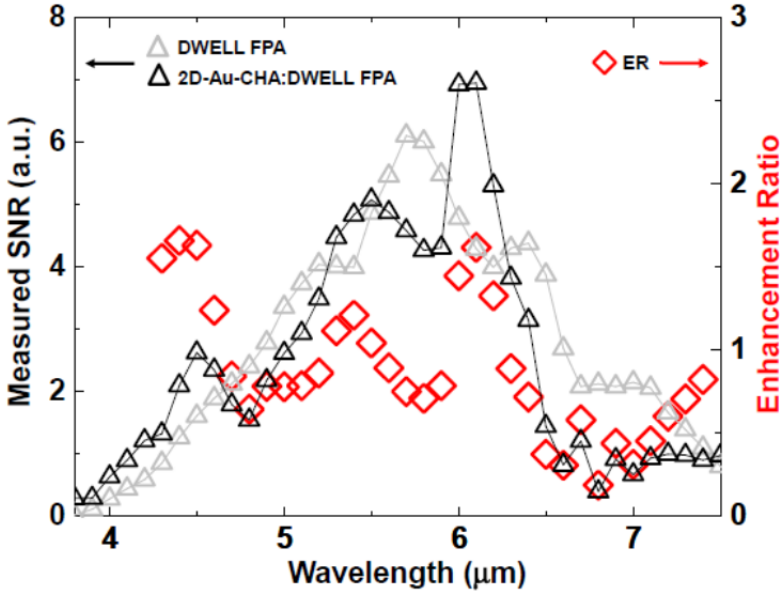


Fig. 4 Experimental SNRs of the DWELL FPA (gray triangle) and 2D-Au-CHA:DWELL FPA (black triangle), and the corresponding enhancement ration (red diamond) by 2D-Au-CHA:DWELL FPA over the DWELL FPA.

Clearly there are resonances at $\sim 4.56 \mu\text{m}$, $\sim 5.45 \mu\text{m}$, and $\sim 6.38 \mu\text{m}$. It is of great importance to investigate the electric field distributions in the effective absorber at resonant wavelengths because the absorption is related to the orientation and intensity of electric fields as shown in Eq. (1) and the effective absorber is especially sensitive to E_z due to η . In addition, understanding this mechanism helps us to improve the design of the perforated metal film integrated infrared FPA. At $4.56 \mu\text{m}$ and $6.38 \mu\text{m}$, E_x distribution in z direction is not due to the propagating modes shown in perforated metal film integrated front-illuminated device, but rather to the guided Fabry-Perot modes resulting from the presence of metal ground plane in the FPA structure; E_z distribution in the plane parallel to the perforated metal film exhibits the SPP modes (1st and 2nd order SPPs owing to the interaction between the first and second nearest apertures, respectively); E_z in z direction displays the exponential decay of a surface wave as shown in the insets of Fig. 3. The responsivity at $5.45 \mu\text{m}$ is increased by the guided Fabry-Perot mode, evidenced by a standing wave pattern of E_x along z direction depicted in the inset of Fig. 3.

To accurately quantify the resonant enhancement, we consider the SNRs of 2D-Au-CHA:DWELL FPA and DWELL FPA. The signal is the intensity of averaged spectral response and the noise is the standard deviation of spectral response over 20 frames. Subsequently, the SNRs of 2D-Au-CHA:DWELL FPA and DWELL FPA were computed and shown in Fig. 4 for the entire wavelength range. By taking the ratio between the SNRs of 2D-Au-CHA:DWELL FPA and DWELL FPA, we extracted three enhancement ratios, 1.63 ($4.5 \mu\text{m}$), 1.21 ($5.5 \mu\text{m}$), and 1.59 ($6.1 \mu\text{m}$) by 2D-Au-CHA:DWELL FPA, respectively. The overall agreement between experimental results and the simulated enhancement ratios at the corresponding resonance is

apparent from Fig. 3. Error in resonance wavelengths between simulation and experiment, $\Delta\lambda = (\lambda_{\text{sim}} - \lambda_{\text{exp}})/\lambda_{\text{exp}}$, is less than 5%, which can be attributed to imperfections and variation from the fabrication process. The enhancement ratios over the full spectrum are shown in Fig. 4.

In addition, the NEDT for 2D-Au-CHA:DWELL FPA at a device temperature of 77 K was measured by changing the irradiance via a calibrated blackbody source at various scene temperatures. By definition, the NEDT (in units of mK) is a performance measure of FPA's sensitivity which indicates the smallest uniform scene temperature difference the FPA can detect. In the measurement setup, we used a narrowband optical filter centered at 5.95 μm with $\Delta\lambda \sim 140$ nm in front of the blackbody source for demonstrating the sensitivity enhancement near the first resonance. NEDT values were obtained by using the FPA's output response (ΔV_0) between two temperatures of the blackbody source (ΔT), along with the recorded noise (V_n) at the lower temperature with the following equation [20–22]: $\text{NEDT} = \Delta T/(\Delta V_0/V_n)$. We computed the NEDT averaged over 121 uniform and well-behaved pixels on the array. The averaged NEDTs of 2D-Au-CHA:DWELL FPA and DWELL FPA were 77.3 mK and 109.1 mK at an irradiance of $3.65 \times 10^{-5} \text{ W/cm}^2$. By comparison, this corresponds to a sensitivity improvement of 2D-Au-CHA:DWELL FPA by a factor of 1.4 over DWELL FPA.

5. CONCLUSIONS

In summary, we have investigated the effect of 2D-Au-CHA on the performance of an infrared DWELL FPA both numerically and experimentally. The wavelength selective enhancement due to the 2D-Au-CHA (or perforated metal film) in an infrared FPA could have a dramatic impact on multispectral (or hyperspectral) imaging system construction. Understanding the underlying mechanism by means of a simulation may offer the possibility to explore a large variety of phenomena in the next generation of infrared detectors associated with surface plasmon polariton and guided Fabry-Perot modes, as well as applications in polarimetric infrared imaging and the improvement of the design of infrared detectors integrated with any type of couplers. A useful result is that the enhanced electric fields inside the effective absorber are strongly associated with the thickness of contact layer and QD layer (i.e., spacer between perforated metal film and metal ground plane), therefore additional design and fabrication refinement are needed for better performance of the perforated metal film integrated FPA.

REFERENCES

1. V. Ryzhii, "The theory of quantum-dot infrared phototransistors," *Semicond. Sci. Technol.* 11(5), 759–765 (1996).
2. S. Krishna, S. D. Gunapala, S. V. Bandara, C. Hill, and D. Z. Ting, "Quantum Dot Based Infrared Focal Plane Arrays," *Proc. IEEE* 95(9), 1838–1852 (2007).
3. P. Boucaud and S. Sauvage, "Infrared photodetection with semiconductor self-assembled quantum dots," *C. R. Phys.* 4(10), 1133–1154 (2003).
4. G. T. Liu, A. Stintz, H. Li, T. C. Newell, G. L. Gray, P. M. Varangis, K. J. Malloy, and L. F. Lester, "The Influence of Quantum-Well Composition on the Performance of Quantum Dot Lasers Using InAs/InGaAs Dots-in-a-Well (DWELL) Structures," *IEEE J. Quantum Electron.* 36(11), 1272–1279 (2000).
5. A. Rogalski, J. Antoszewski, and L. Faraone, "Third-generation infrared photodetector arrays," *J. Appl. Phys.* 105(9), 091101 (2009).
6. C. Genet and T. W. Ebbesen, "Light in tiny holes," *Nature* 445(7123), 39–46 (2007).
7. D. Wasserman, E. A. Shaner, and J. G. Cederberg, "Midinfrared doping-tunable extraordinary transmission from sub-wavelength Gratings," *Appl. Phys. Lett.* 90(19), 191102 (2007).
8. C.-C. Chang, Y. D. Sharma, Y.-S. Kim, J. A. Bur, R. V. Shenoi, S. Krishna, D. Huang, and S.-Y. Lin, "A Surface Plasmon Enhanced Infrared Photodetector Based on InAs Quantum Dots," *Nano Lett.* 10(5), 1704–1709 (2010).
9. S. C. Lee, Y. D. Sharma, S. Krishna, and S. R. J. Brueck, "Leaky-mode effects in plasmonic-coupled quantum dot infrared photodetectors," *Appl. Phys. Lett.* 100(1), 011110 (2012).
10. J. Rosenberg, R. V. Shenoi, T. E. Vandervelde, S. Krishna, and O. Painter, "A multispectral and polarization-selective surface-plasmon resonant midinfrared detector," *Appl. Phys. Lett.* 95(16), 161101 (2009).
11. S. J. Lee, Z. Ku, A. Barve, J. Montoya, W.-Y. Jang, S. R. J. Brueck, M. Sundaram, A. Reisinger, S. Krishna, and S. K. Noh, "A monolithically integrated plasmonic infrared quantum dot camera," *Nat. Commun.* 2, 286 (2011).
12. M. G. Moharam and T. K. Gaylord, "Rigorous coupled-wave analysis of planar-grating diffraction," *J. Opt. Soc. Am.* 71(7), 811–818 (1981).
13. I. N. Stranski and L. Krastanow, "Sitzungsberichte d. Akad. D. Wissenschaften in Wien," *Abt. IIb, Band 146*, 797–810 (1937).
14. D. Xia, Z. Ku, S. C. Lee, and S. R. J. Brueck, "Nanostructures and Functional Materials Fabricated by Interferometric Lithography," *Adv. Mater. (Deerfield Beach Fla.)* 23(2), 147–179 (2011).
15. M. A. Ordal, L. L. Long, R. J. Bell, S. E. Bell, R. R. Bell, R. W. Alexander Jr, and C. A. Ward, "Optical properties of the metals Al, Co, Cu, Au, Fe, Pb, Ni, Pd, Pt, Ag, Ti, and W in the infrared and far infrared," *Appl. Opt.* 22(7), 1099–20 (1983).
16. W. G. Spitzer and J. M. Whelan, "Infrared Absorption and Electron Effective Mass in n-Type Gallium Arsenide," *Phys. Rev.* 114(1), 59–63 (1959).
17. A. Barve, T. Rotter, Y. Sharma, S. J. Lee, S. K. Noh, and S. Krishna, "Systematic study of different transitions in high operating temperature quantum dots in a well photodetectors," *Appl. Phys. Lett.* 97(6), 061105 (2010).
18. J. D. Jackson, *Classical Electrodynamics* (Wiley, New York, 3rd Edition, 1999).

19. J. O. Kim, S. Sengupta, A. V. Barve, Y. D. Sharma, S. Adhikary, S. J. Lee, S. K. Noh, M. S. Allen, J. W. Allen, S. Chakrabarti, and S. Krishna, "Multi-stack InAs/InGaAs Sub-monolayer Quantum Dots Infrared Photodetectors," *Appl. Phys. Lett.* 102(1), 011131 (2013).
20. E. L. Dereniak and G. Boreman, *Infrared Detectors and Systems* (Wiley, 1996).
21. T. E. Vandervelde, M. C. Lenz, E. Varley, A. Barve, J. Shao, R. Shenoi, D. A. Ramirez, W.-Y. Jang, Y. D. Sharma, and S. Krishna, "Quantum Dots-in-a-Well Focal Plane Arrays," *IEEE J. Sel. Top. Quantum Electron.* 14(4), 1150–1161 (2008).
22. J. R. Andrews, S. R. Restaino, S. W. Teare, Y. D. Sharma, W.-Y. Jang, T. E. Vandervelde, J. S. Brown, A. Reisinger, M. Sundaram, S. Krishna, and L. Lester, "Comparison of Quantum Dots-in-a-Double-Well and Quantum Dots-in-a-Well Focal Plane Arrays in the Long-Wave Infrared," *IEEE Trans. Electron. Dev.* 58(7), 2022–2027 (2011).

LIST OF ABBREVIATIONS

DWELL	Dots-in-a-well
DDWELL	Dots-in-a-double well
FPAs	Focal Plane Arrays
InAs	Indium Arsenide
MBE	Molecular Beam Epitaxy
NEDT	Noise Equivalent Difference in Temperature
QDs	Quantum dots
QW	Quantum well
SNR	Signal to noise
SP	Surface Plasmon
SPP	Surface Plasmon Polariton

DISTRIBUTION LIST

DTIC/OCF	
8725 John J. Kingman Rd, Suite 0944	
Ft Belvoir, VA 22060-6218	1 cy
AFRL/RVIL	
Kirtland AFB, NM 87117-5776	2 cys
Official Record Copy	
AFRL/RVSS/David Cardimona	1 cy